

Compression-thinning behavior of bubble suspensions

Hu Sun,¹ Qingfei Fu,^{1,2,3,*} Chiyu Xie,^{1,2} Bingqiang Ji,^{1,2,†} and Lijun Yang^{1,2,3,‡}

¹*School of Astronautics, Beihang University, Beijing 100191, PR China*

²*Aircraft and Propulsion Laboratory, Ningbo Institute of Technology,
Beihang University, Ningbo 315800, PR China*

³*National Key Laboratory of Aerospace Liquid Propulsion, Xi'an 710100, PR China*

Rheology of bubble suspensions is critical for the prediction and control of bubbly flows in a wide range of industrial processes. It is well-known that the bubble suspension exhibits a shear-thinning behavior due to the bubble shape deformation under pure shear, but how the shear rheology response to dilatation remains unexplored. Here, we report a compression-thinning behavior that the bubble suspension exhibits a decreasing shear viscosity upon compressing. This peculiar rheological behavior is microscopically due to that a shrinking bubble surface effectively weakens the flow resistance of the surrounding liquid. We theoretically propose a constitutive equation for dilute bubble suspensions considering both shear and dilatation effects, and demonstrate that the contribution of dilatation effect on the shear viscosity can be significant at a changing pressure.

I. INTRODUCTION

Bubbly flows pervade a wide range of industrial processes in geological, chemical, pharmaceutical, and food engineering [1, 2]. Though the continuous liquid phase is Newtonian, the introduction of discrete bubbles endows the dispersion system with complex non-Newtonian behaviors such as shear-dependent viscosity and elasticity [3–6], producing challenges to the prediction and control of the flow behaviors. Originating with the well-known Einstein equation [7, 8], rheological models of bubble suspensions have been established with a special focus on the shear viscosity [9–14], where bubbles are regarded as special incompressible “inviscid droplets”. These models predict the shear-thinning and relaxation behavior of bubble

* fuqingfei@buaa.edu.cn

† bingqiangji@buaa.edu.cn

‡ yanglijun@buaa.edu.cn

suspensions, which has been confirmed by experiments with simple shear flows [15–20].

However, different from droplets, bubbles are highly compressible. Taylor pointed out that the presence of bubbles makes the suspension compressible and results in a dilatational viscosity [21]. Thus, dilatation motion will be triggered in bubbly flows due to the violent pressure variations in practical scenarios such as foam flooding and fuel injection [22–26]. In fact, the expansion or compression of bubbles change the shear flow field by introducing an additional centripetal flow and affecting their shape deformation [27–30], and thus may modify the shear rheological properties of the suspension. Unfortunately, due to the incompressible assumption of bubbles, previous models fundamentally ignored the contribution of dilatation motion on the suspension’s shear viscosity [10, 11]. How the shear rheology of bubble suspensions response to dilatation remains unexplored.

In this work, we theoretically develop a novel constitutive equation for dilute bubble suspensions undergoing a motion of both shear and dilatation. We reported a compression-thinning behavior, a distinct rheological property endowed by bubble compressibility upon a changing pressure, which can significantly influence the suspensions’ shear viscosity. Our study highlight the critical role of dilatation motion in mediating the shear rheology of bubble suspensions.

II. CONSTITUTIVE EQUATION

We consider the shear rheology of a fluid element of a dilute suspension with length scales much larger than the bubble size, where the relationship between the bulk stress and the bulk rate-of-strain tensor is established by Batchelor’s volume averaging method [31], which gives

$$\langle \boldsymbol{\tau} \rangle = 2\mu_l \langle \mathbf{e} \rangle + \frac{N}{V} \boldsymbol{\Sigma}^g, \quad (1)$$

where $\langle \cdot \rangle$ marks averaged parameters in the fluid element, $\boldsymbol{\tau}$ is the deviatoric stress tensor, \mathbf{e} is the rate-of-strain tensor, μ_l is the viscosity of the liquid phase which is Newtonian here. V is the element volume, and N is the bubble number. For simplicity, the bubbles in the fluid element are assumed to be monodisperse without interactions between each other. Based

on Gauss's law, the stress contribution of an individual bubble, Σ^g , is written as [31]

$$\Sigma^g = \int_S \mathbf{n} \cdot (\boldsymbol{\sigma}_l \mathbf{r}) - \frac{1}{3} (\boldsymbol{\sigma}_l : \mathbf{n} \mathbf{r}) \boldsymbol{\delta} - \mu_l (\mathbf{n} \mathbf{u}_l + \mathbf{u}_l \mathbf{n}) dS, \quad (2)$$

where the subscripts l and g respectively denote the liquid and gas phases, \mathbf{n} and \mathbf{r} respectively represent the unit outer normal vector and the position vector on the surface S , $\boldsymbol{\sigma}$ and \mathbf{u} respectively represent the stress tensor and local velocity vector, $\boldsymbol{\delta}$ is the Kronecker tensor.

To evaluate the influence of bubbles to the macroscopic rheological properties, we consider the microscopic flow of a fluid element containing a small bubble of equivalent initial radius a , with a macroscopic velocity \mathbf{U} , pressure P , shear rate $\dot{\gamma}$, and rate of change in pressure dP/dt . In the following, we make all parameters dimensionless using a , $\dot{\gamma}^{-1}$, and $\mu_l \dot{\gamma}$ as the characteristic length, time, and stress scales, respectively. The liquid flow around the bubble is described by the Stokes equation considering the low Reynolds number [32],

$$\nabla \cdot \mathbf{u}_l = 0, \quad \nabla p_l = \nabla^2 \mathbf{u}_l, \quad (3)$$

and the gas in the bubble is assumed to be compressible, inviscid, and ideal, yielding

$$\nabla \cdot \mathbf{u}_g = -\frac{1}{p_g} \frac{dp_g}{dt}, \quad \nabla p_g = 0, \quad (4)$$

where ∇ is the Hamiltonian operator and p is the local pressure.

We describe the velocities, stresses, and the bubble deformations explicitly through spherical harmonic analysis. The solutions to Stokes Equations [Eq. (3)] were given by Lamb [33], and the velocity inside the bubble is derived as

$$\mathbf{u}_g = -\frac{1}{6p_g} \frac{dp_g}{dt} \nabla r^2 + \sum_{n=0}^{+\infty} \nabla (r^n \mathcal{Y}_n^g), \quad (5)$$

where $r = |\mathbf{r}|$, and \mathcal{Y}_n^g is a spherical surface harmonic of order n (see Appendix A and B for details of the theoretical derivations and expressions).

At the bubble surface separating the gas and liquid phases, the free slip boundary condition gives $(\boldsymbol{\delta} - \mathbf{nn}) \cdot \boldsymbol{\sigma}_l \cdot \mathbf{n} = 0$, and the normal stress balance gives $\boldsymbol{\sigma}_l : \mathbf{nn} - \boldsymbol{\sigma}_g : \mathbf{nn} = Ca_S^{-1} (R_1^{-1} + R_2^{-1})$, the normal velocity continuity gives $\mathbf{u}_l \cdot \mathbf{n} = \mathbf{u}_g \cdot \mathbf{n}$. Here, $Ca_S = \mu_l a \dot{\gamma} / \Gamma$

is the shear capillary number comparing the shear-induced viscosity to capillarity, R_1 and R_2 are the principle radii of curvature of the interface (Appendix C). The harmonic expressions of the velocities and stresses can be theoretically solved combining with the above boundary conditions, once we know the equation of the bubble surface.

The equation of bubble surface is expressed by considering an additional deformation caused by the rate of change in pressure, $Ca_D f^D$, on a certain initial shape $f^{(0)}$, i.e.,

$$r = f^{(0)} + Ca_D f^D, \quad (6)$$

where $f^{(0)}$ is given by Frankel's model [11] as $f^{(0)} = 1 + Ca_S \mathcal{F}^S$ (Appendix D), and Ca_D is the dilatation capillary number defined as

$$Ca_D = -\frac{\mu_l a}{\Gamma} \frac{dP}{P dt}, \quad (7)$$

comparing the dilatation-induced viscosity to capillarity, which is positive upon decompressing and negative upon compressing. f^D is also expressed using surface harmonics as $f^D = \sum \mathcal{F}_n^D$ ($n \geq 0$) (Appendix D).

To analytically solve the above equations, we assume the bubble shape deformation and volume dilatation are small ($Ca_S < 1$ and $Ca_D < 1$), thus yielding an influence to the flow belongs to $O(Ca)$. Then the surface harmonics can be solved by the regular perturbation method [11, 32]. Results show that only the 0th- and 2nd-order surface harmonics should be considered with the high orders negligible in comparison. Finally, the liquid velocity around the bubble is solved as (Appendix A)

$$\mathbf{u}_l = \mathbf{U} + \nabla (r^{-1} \mathcal{Y}_0^l + r^{-3} \mathcal{Y}_2^l) + \frac{1}{2} r^{-3} \mathcal{Z}_2^l \mathbf{r}, \quad (8)$$

where \mathcal{Y}_n^l is different surface harmonics corresponding to the velocity field of the liquid stokes flow, and \mathcal{Z}_2^l is the second order surface harmonics of the liquid pressure, expressed as $\mathcal{Z}_2^l = 3\mathbf{Z}^l : \mathbf{r}\mathbf{r}r^{-2}$, where

$$\mathbf{Z}^l = -\frac{2}{3}\mathbf{E} + Ca_S \mathbf{Z}_S^l + Ca_D \mathbf{Z}_D^l. \quad (9)$$

On the right hand of Eq. (9), the first term represents the influence of spherical bubbles with

$\mathbf{E} = \frac{1}{2}(\nabla\mathbf{U} + \mathbf{U}\nabla)$ [9], the second term considers the influence of bubble shape deformation under pure shear [11], and the third term evaluates the contribution of bubble volume dilatation with

$$\mathbf{Z}_D^l = -2\mathcal{F}_0^D\mathbf{E} - \frac{8}{15}\dot{R}\mathbf{E}, \quad (10)$$

where $R = 1 + Ca_D\mathcal{F}_0^D$ is the equivalent radius of the deformed bubble at time t , which equals to 1 at $t = 0$. $\dot{R} = dR/dt$ represents the average expansion speed of the bubble surface.

Then, the dimensionless tress contribution of the bubble is obtained as Eq. (11), by substituting the solutions of velocities and stresses into Eq. (2).

$$\Sigma^g = -\frac{8\pi R^3}{9}(\nabla \cdot \mathbf{u}_g)\boldsymbol{\delta} - 4\pi\mathbf{Z}^l, \quad (11)$$

where $\nabla \cdot \mathbf{u}_g$ is the average velocity divergence of the gas phase. At a sufficient large pressure that overwhelms the capillary and viscous stresses at the bubble surface, p_g approximately equals P (Appendix E), and thus

$$\nabla \cdot \mathbf{u}_g = -\frac{1}{P} \frac{dP}{dt}. \quad (12)$$

This means that the volumetric dilatation rate [34] of the suspension can be expressed as $\dot{\mathcal{V}} = -\phi dP/(Pdt)$ where $\phi = \phi_0[1 + tdP/(Pdt)]^{-1}$ is the void fraction of the dilute suspension at time t , and the dilatation capillary number can also be expressed as $Ca_D = \mu_l a \dot{\mathcal{V}}/(\Gamma\phi)$.

Substituting Eq. (11) into Eq. (1), we obtain the constitutive equation of the bubble suspension as

$$\langle \boldsymbol{\tau} \rangle = 2(1 + \phi) \langle \hat{\mathbf{e}} \rangle + \langle \boldsymbol{\tau}_S \rangle + \langle \boldsymbol{\tau}_D \rangle, \quad (13)$$

where $\hat{\mathbf{e}}$ is the deviatoric rate-of-strain tensor, and $1 + \phi$ in the first term on the left hand is the relative viscosity derived by Taylor with spherical bubble assumption [9]. $\langle \boldsymbol{\tau}_S \rangle$ evaluates the stress contribution of bubble shape deformation caused by the pure shear flow, given by Frankel & Acrivos [11] as

$$\langle \boldsymbol{\tau}_S \rangle = \phi Ca_S \left(-\frac{32}{5} \frac{\mathcal{D} \langle \hat{\mathbf{e}} \rangle}{\mathcal{D}t} + \frac{48}{35} \mathcal{L} [\langle \hat{\mathbf{e}} \rangle \cdot \langle \hat{\mathbf{e}} \rangle] \right), \quad (14)$$

where $\mathcal{D}/\mathcal{D}t$ is the Jaumann derivative, and $\mathcal{L}[\cdot]$ indicates that only the deviatoric part is

retained.

The last term of Eq. (13), $\langle \boldsymbol{\tau}_D \rangle$, represents the stress contribution of the bubble volume dilatation due to the rate of change in pressure, which is expressed as

$$\langle \boldsymbol{\tau}_D \rangle = \frac{8}{15} \phi C a_D \langle \hat{\mathbf{e}} \rangle, \quad (15)$$

influenced by the volumetric dilatation rate instead of the dilatation amount. Eq. (13) indicates that the shear rheology of the dilute bubble suspension is determined by the current void fraction ϕ , $C a_S$, and $C a_D$. When there is no significant pressure variation, $C a_D \approx 0$, and Eq. (13) reduces to Frankel & Acrivos equation [11], which served as the origin of several followed constitutive equations for bubble suspensions [4, 20]. However, the suspension undergoes dilatation motion upon pressure variation due to the bubble compressibility. Our new constitutive equation demonstrates that the bubble compressibility decreases the viscosity when the pressure is increasing ($C a_D < 0$), referring to compression-thinning effect, while it increases the viscosity at decreasing pressure ($C a_D > 0$), referring to decompression-thickening effect. Indeed, the volumetric dilatation rate modifies the suspensions' shear rheological properties, endowed by the intrinsic compressibility of the gas bubbles, which has not been realized in previous studies on shear rheology of bubble suspensions to our best knowledge.

III. RESULT AND DISCUSSION

To unveil the behind physics of the compression-thinning behavior caused by bubble compressibility, we analyze the microscopic flow field around a single bubble under a steady shear (Fig. 1). We found that a changing pressure does not apparently affect the bubble shape, but it significantly changes the velocity field around the bubble. The disturbance of the bubble to the liquid flow field only manifests near the bubble, and quickly decays, becoming negligible at a distance of a away from the bubble surface. Without volume dilatation, the liquid flows around the bubble surface, with a zero normal velocity at the interface [Fig. 1(a)]. Thus, the bubble acts like an inviscid droplet, and the macroscopic shear viscosity of the suspension is only influenced by the bubble shape and volume fraction, depending on $C a_S$ and ϕ_0 respectively. The presence of bubble leads to the deflection of the

liquid streamlines and increases flow resistance, usually resulting a viscosity larger than the liquid viscosity at $Ca_S < 1$ [9, 13, 16]. When the pressure is changing, the bubble surface is expanding or shrinking due to the volume dilatation, exerting the liquid near the bubble surface a velocity normal to the interface and allowing the liquid streamlines cross the bubble surface. Specifically, the expanding interface at decreasing pressure forces the external fluid to flow toward the outer layer [Fig.1(b)]. As a result, the external shear flow is subject to an additional repulsion when approaching the bubbles, which will lead to greater deflection of the liquid streamlines and a stronger flow resistance, thus resulting in a decompression-thickening effect. On the contrary, the shrinking interface at increasing pressure leads to weaker deflection of the liquid streamlines and a smaller flow resistance [Fig.1(c)], yielding a compression-thinning effect. This compression-thinning behavior is thus determined by the rate of bubble volume dilatation, characterized by the dilatation capillary number Ca_D .

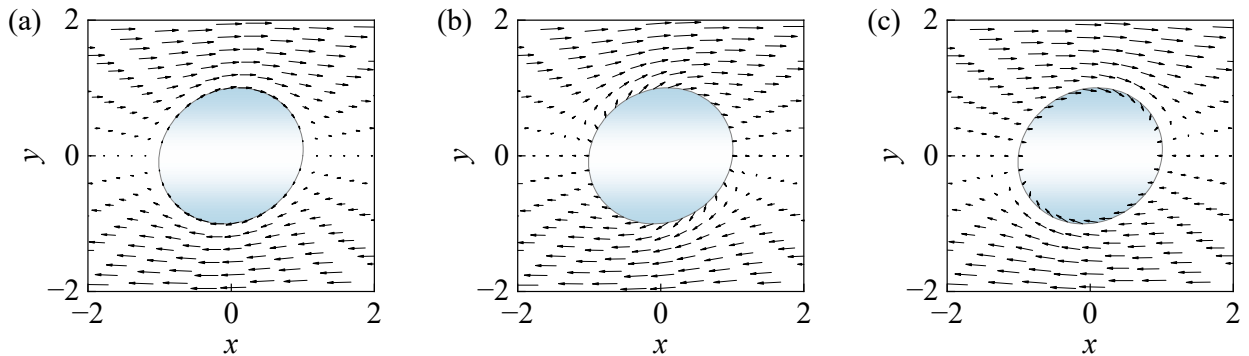


FIG. 1. Velocity field of the liquid surrounding a bubble undergoing a shear flow ($Ca_S = 0.05$) with (a) $Ca_D = 0$, (b) $Ca_D = 0.05$ (decompressing) and (c) $Ca_D = -0.05$ (compressing). The shade region represents the middle cross section of the bubble at the direction perpendicular to the shear plane. The black arrows represent the liquid velocity vectors.

We then quantify the contribution of the bubble compressibility to the suspension's shear rheology. With a pressure changing with time, the stress relaxation behavior need to be considered in the shear rheology by applying the operator $(1 + \lambda_t \mathcal{D}/Dt)$ to Eq.(13) [4, 5, 20], where $\lambda_t = 6Ca_S/5$ is the stress relaxation time. Due to the volume dilatation at a changing pressure, the time derivative of the volume fraction $d\phi/dt = \dot{\mathcal{V}}$ is considered. Then the time evolution of the suspension viscosity can be obtained once we know the ϕ_0 , Ca_S , and Ca_D at the initial moment (Appendix F). Referring to the parameter ranges in the displacement or pipeline transport processes of foamy oil reported in previous experiments

where significant pressure variations exist [24, 35–37], we consider $\mu_l = 5 \text{ Pa} \cdot \text{s}$, $\Gamma = 50 \text{ mN/m}$, $a = 10\text{-}10^3 \mu\text{m}$, $\dot{\gamma} = 1\text{-}100 \text{ s}^{-1}$, $P = 1\text{-}10 \text{ bar}$, $|dP/dt| \leq 3 \text{ bar/s}$, which corresponds to a $Ca_S = 10^{-4}\text{-}10$ and $Ca_D \sim O(10^{-1})$. To differentiate the viscosity contributions from different mechanisms, we express the relative viscosity of the suspension ($\mu_r = \mu/\mu_l$) as $\mu_r = 1 + \Delta\mu_r^T + \Delta\mu_r^S + \Delta\mu_r^D$, where $\Delta\mu_r^T = \phi$ is the shear-independent viscosity derived by Taylor [21], $\Delta\mu_r^S$ is the pure shear induced viscosity evaluating the real time contribution from a pure steady shear proposed by Frankel & Acrivos [11], and $\Delta\mu_r^D$ is the dilatation induced viscosity under a changing pressure, as a viscosity correction resulted from the dilatation motion.

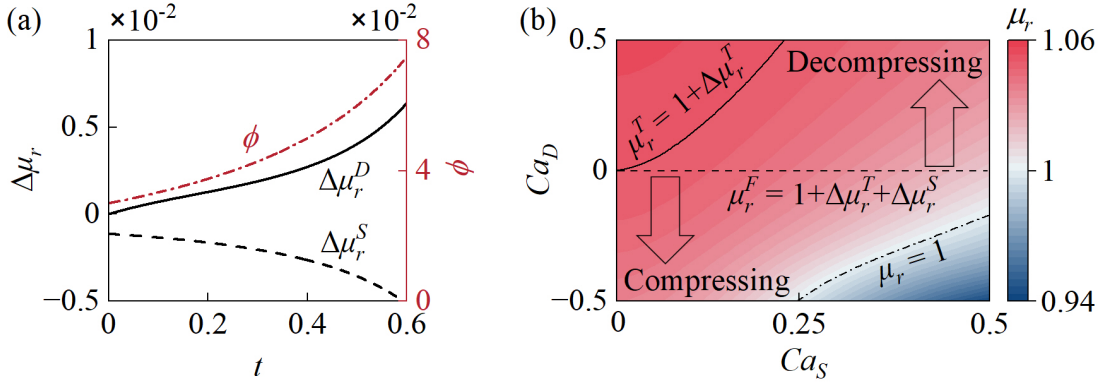


FIG. 2. (a) Time evolution of the relative viscosity μ_r and void fraction ϕ for a bubble suspension of $\phi_0 = 0.03$ at $Ca_S = Ca_D = 0.1$. $\Delta\mu_r^S$ is the pure shear induced viscosity correction [11], and $\Delta\mu_r^D$ is the dilatation induced viscosity correction we proposed. (b) μ_r of the same suspension at the moment when it expands to $\phi = 0.05$ at different Ca_S and Ca_D . μ_r^T and μ_r^F are respectively the theoretical predictions by Taylor [21] and Frankel & Acrivos [11].

Fig. 2(a) shows the time evolution of μ_r for a suspension of $\phi_0 = 0.03$, suffering from a constant $\dot{\gamma}$ and a negative dP/dt with $Ca_S = Ca_D = 0.1$. The void fraction ϕ as well as $\Delta\mu_r^T$ increases with time upon decompressing as $\phi = \phi_0[1 + tdP/(Pdt)]^{-1}$. The pure shear induced viscosity $\Delta\mu_r^S$ exhibits a negative correction because the bubble shape deformation facilitates a smaller flow resistance, yielding a shear-thinning effect. In contrast, the dilatation induced viscosity $\Delta\mu_r^D$ shows a positive correction due to the enhanced flow resistance caused by bubble surface expansion. $\Delta\mu_r^D$ and $\Delta\mu_r^S$ both increase with increasing ϕ with similar magnitudes, and $\Delta\mu_r^D$ even exceeds $\Delta\mu_r^S$ in the later stage of expansion. The relative viscosity of the same suspension at the moment when it expands to $\phi = 0.05$ with different Ca_S and Ca_D are presented in Fig. 2(b). Generally, μ_r decreases with Ca_S and increases

with Ca_D , caused by the different physics behind the viscosity correction induced by pure shear and dilatation. Compared to the viscosity calculated by the equation of Frankel & Acrivos ($\mu_r^F = 1 + \Delta\mu_r^T + \Delta\mu_r^S$) without considering dilatation effect [11], the μ_r calculated by our model increases with the decompressing rate and decreases with the compressing rate, highlighting the compression-thinning or decompression-thickening behavior stemmed from the dilatation motion of the suspension endowed by bubble compressibility. At a large $|Ca_D|$, this dilatation induced rheological effect can play a leading role in the shear viscosity of the suspension, yielding a μ_r larger than Taylor's prediction ($1 + \phi$) at a large decompressing rate and a μ_r smaller than 1 at a large compressing rate.

It seems unexpected that the bubble compressibility can profoundly modify the shear viscosity of the suspension, considering the minor volume dilatation of the dilute suspension of small ϕ . Using the parameter values mentioned before, a Ca_D of 0.1 corresponds to a volumetric dilatation rate of $\dot{\mathcal{V}} = 3\% \text{ s}^{-1}$ for $a = 1 \text{ mm}$ at 1 atm, which means that the volume variation of the bubble suspension is usually unobtrusive at high frequency pressure fluctuations in industry [38, 39]. Exemplified with the significant compression-thinning effect for dilute suspensions upon pressure variation, we highlight the critical role of microscopic flows around the single bubbles in shaping the macroscopic properties of the bubble suspensions. We envision that the shear viscosity contributed by the dilatation motion may be more important for dense bubble suspensions, which remains to be explored in future studies. In addition, we note that the existing rheology experiments are usually conducted at a simple shear flow without violent pressure changing. It is thus interesting to explore the implications of our model by rheological measurements with significant rate of change in pressure regarding the complex flows in practical situations.

IV. CONCLUSION

In summary, we theoretically investigate the shear rheology of dilute bubble suspensions in consideration of the volume dilatation endowed by bubble compressibility. Our constitutive equation reports a compression-thinning behavior for the first time, manifesting a decreasing shear viscosity upon compressing and an increasing shear viscosity upon decompressing. This peculiar behavior is microscopically derived from the fact that the shrinking motion of the bubble surface upon compressing weakens the flow resistance of the external liquid under

shear, and vice versa. We show the dilatation induced viscosity can exceed the shear induced viscosity and dominate the suspension's shear viscosity in practical scenarios. Our study not only advances the understanding on the rheological behaviors of dispersion systems, but also may provide guidance for the flow control of bubble suspensions in practice.

APPENDIX A: SOLUTION OF STOKES LIQUID FLOW BY SPHERICAL HARMONIC ANALYSIS

According to the standard solution of Stokes Equations given by Lamb [33], the local velocity of the liquid phase around the bubble, \mathbf{u}_l , is expressed as

$$\mathbf{u}_l = \mathbf{U} + \sum_{n=0}^{+\infty} \left[\nabla (r^{-n-1} \mathcal{X}_n^l) \times \mathbf{r} + \nabla (r^{-n-1} \mathcal{Y}_n^l) - \frac{n-2}{2n(2n-1)} r^2 \nabla (r^{-n-1} \mathcal{Z}_n^l) + \frac{n+1}{n(2n-1)} \mathbf{r} (r^{-n-1} \mathcal{Z}_n^l) \right], \quad (16)$$

and the local liquid pressure, p_l , is derived as

$$p_l = P + \sum_{n=1}^{+\infty} (r^{-n-1} \mathcal{Z}_n^l). \quad (17)$$

where all parameters are dimensionless, \mathcal{X}_n^l , \mathcal{Y}_n^l and \mathcal{Z}_n^l are three different spherical surface harmonics of order n . According to the orthogonality relations, these three kinds of harmonics can be solved analytically using the regular perturbation method [11, 32], e.g. $\mathbf{u} = \bar{\mathbf{u}} + Ca_S \tilde{\mathbf{u}}_S + Ca_D \tilde{\mathbf{u}}_D$ where the superscripts $\bar{\cdot}$ and $\tilde{\cdot}$ represent the $O(1)$ and $O(Ca)$ components, respectively.

Firstly, the zeroth order harmonics should satisfy the following relationships:

$$\frac{\mathcal{Y}_0^l}{R^3} = -\frac{1}{R} \frac{dR}{dt} = -\frac{1}{3} (\nabla \cdot \mathbf{u}_g), \quad (18)$$

$$p_g = P(t) + 2Ca_S^{-1} \frac{1}{R} + \frac{4}{R} \frac{dR}{dt}, \quad (19)$$

where the equivalent bubble radius R is related to the 0th-order harmonic \mathcal{F}_0^D . According to the ideal gas law and mass conservation, R is determined by the pressure inside the

bubble, which means that $p_g R^3$ is always equal to the initial value $p_g|_{t=0}$. Hence, \mathcal{Y}_0^l and $\nabla \cdot \mathbf{u}_g$, the volumetric dilatation rate of the single bubble, can be obtained accurately by solving the set of differential equations, Eqs. (18) and (19). At a sufficient large pressure that overwhelms the capillary and viscous stresses at the bubble surface, p_g approximately equals P (Appendix E), we have $\nabla \cdot \mathbf{u}_g = -dP/(Pdt)$.

Then the coefficients of the second order harmonics can be derived as

$$\mathbf{Y}^l = Ca_S \left(\frac{2}{15} \frac{D\mathbf{E}}{Dt} - \frac{2}{45} \mathcal{L}[\mathbf{E} \cdot \mathbf{E}] \right) + Ca_D \left(-\frac{8}{45} \mathbf{E} \right), \quad (20)$$

$$\mathbf{Z}^l = -\frac{2}{3} \mathbf{E} + Ca_S \left(\frac{32}{15} \frac{D\mathbf{E}}{Dt} - \frac{48}{105} \mathcal{L}[\mathbf{E} \cdot \mathbf{E}] \right) + Ca_D \left(-2\mathcal{F}_0^D \mathbf{E} - \frac{8}{45} \mathbf{E} \right), \quad (21)$$

and the second order harmonics is obtained by $\mathcal{Y}_2^l = 3\mathbf{Y}^l : \mathbf{r}\mathbf{r}\mathbf{r}^{-2}$ and $\mathcal{Z}_2^l = 3\mathbf{Z}^l : \mathbf{r}\mathbf{r}\mathbf{r}^{-2}$. The odd order harmonics are zero and the harmonics with an order larger than 2 is negligible compared to the zeroth and second orders.

APPENDIX B: SOLUTION OF THE GAS VELOCITY INSIDE THE BUBBLE BY SPHERICAL HARMONIC ANALYSIS

The velocity potential Φ_g for the inviscid gas is used to describe the velocity inside the bubble, that is $\nabla \Phi_g = \mathbf{u}_g$. Hence,

$$\nabla^2 \Phi_g = -\frac{1}{p_g} \frac{dp_g}{dt}. \quad (22)$$

Assume that the solution of this non-homogeneous differential equation [Eq. (22)] can be expressed as the sum of a general solution θ_g and a special solution ϑ_g , yielding

$$\Phi_g = \theta_g + \vartheta_g, \quad (23)$$

where $\nabla^2 \theta_g = 0$ and $\nabla^2 \vartheta_g = -dp_g/p_g dt$. According to the solution of Laplace Equation, the general solution θ_g can be directly expressed by the spherical surface harmonics, i.e. $\theta_n^g = r^n \mathcal{Y}_n^g$. Meanwhile, since the pressure inside the bubble is independent of the spatial position, as given by $\nabla p_g = 0$, the special solution ϑ_g can be written as $-r^2 dp_g/6p_g dt$.

Hence, the velocity inside the bubble is finally expressed as

$$\mathbf{u}_g = -\frac{1}{6p_g} \frac{dp_g}{dt} \nabla r^2 + \sum_{n=0}^{+\infty} \nabla (r^n \mathcal{Y}_n^g). \quad (24)$$

Through the perturbation method, we obtain $\mathcal{Y}_n^g = 0$ for $n \neq 2$, and $\mathcal{Y}_2^g = 3\mathbf{Y}^g : \mathbf{r}\mathbf{r}r^{-2}$, where

$$\mathbf{Y}^g = Ca_D \left(-\frac{1}{9} \mathbf{E} \right). \quad (25)$$

APPENDIX C: SUM OF THE PRINCIPAL CURVATURES OF THE BUBBLE SURFACE

According to the tensor analysis method [40], the sum of the principle curvatures can be expressed as

$$R_1^{-1} + R_2^{-1} = 2 - 2\Sigma Caf - \Sigma Caf_{,kk} + 2(\Sigma Caf)^2 + 2(\Sigma Caf)(\Sigma Caf_{,kk}) + O(Ca^3), \quad (26)$$

where ΣCaf represents any small deformation of the bubble surface based on the sphere ($r = 1$), and the subscripts comma and kk respectively denote the derivation operator and Einstein summation convention in tensor analysis.

The above equation can be rewritten in the form of spherical surface harmonics, yielding

$$\begin{aligned} R_1^{-1} + R_2^{-1} = & 2 + 4Ca_S \mathcal{F}^S + Ca_D \sum_{n=0}^{+\infty} (n^2 + n - 2) \mathcal{F}_n^D \\ & - 10Ca_S^2 (\mathcal{F}^S)^2 - 2Ca_S Ca_D \mathcal{F}^S \sum_{n=0}^{+\infty} (n^2 + n + 4) \mathcal{F}_n^D \\ & - 2Ca_D^2 \sum_{n=0}^{+\infty} \mathcal{F}_n^D \sum_{n=0}^{+\infty} (n^2 - n - 1) \mathcal{F}_n^D + O(Ca^3), \end{aligned} \quad (27)$$

where $\mathcal{F}_{n,kk} = -n(n+1)\mathcal{F}_n$ can be derived from the Laplace Equation at $r = 1$ [32].

**APPENDIX D: EQUATION OF BUBBLE SURFACE BY SPHERICAL
HARMONICS ANALYSIS**

In Frankel's model [11], the bubble shape under pure shear can be described as $r = 1 + Ca_S \mathcal{F}^S = 1 + 3Ca_S \mathbf{F}^S : \mathbf{r} \mathbf{r} r^{-2}$, where

$$\mathbf{F}^S + \frac{6}{5} Ca_S \frac{\mathcal{D}\mathbf{F}^S}{\mathcal{D}t} = \frac{2}{3} \mathbf{E} + \frac{128}{105} Ca_S \mathcal{L}[\mathbf{E} \cdot \mathbf{E}]. \quad (28)$$

Considering a macroscopic pressure P changing in time, the additional deformation $Ca_D f^D$ due to the bubble compressibility is expressed as the sum of the 0th- and 2nd-order surface harmonics, $Ca_D \mathcal{F}_0^D$ and $Ca_D \mathcal{F}_2^D$, which respectively represent the volume dilatation and additional shape deformation of the bubble. For the former, \mathcal{F}_0^D can be linked to the equivalent radius R , given by $R = \sqrt[3]{P|_{t=0}/P}$. For the latter, the coefficient tensor of \mathcal{F}_2^D is determined by the following differential equation:

$$\mathbf{F}^D + \frac{6}{5} Ca_S \frac{\partial \mathbf{F}^D}{\partial t} = \frac{4}{3} Ca_S \mathcal{F}_0^D \mathbf{E} - \frac{4}{15} Ca_S \mathbf{E}. \quad (29)$$

From Eqs. (28) and (29), we can find that the leading factor is determined by the $O(1)$ component in Eq. (28), that is $2\mathbf{E}/3$, and the relaxation time λ_t is only related to the shear capillary number, i.e. $\lambda_t = 6Ca_S/5$. Hence, the bubble shape is still led by the shear effect in the flow field (Figure 1 in the main text).

For simplicity, these differential equations can be simplified by the successive substitution method [11], as the magnitude of the time derivative terms in Eqs. (28) and (29) are usually less than unity. Thus

$$\mathbf{F}^S = \frac{2}{3} \mathbf{E} + Ca_S \left(-\frac{4}{5} \frac{\mathcal{D}\mathbf{E}}{\mathcal{D}t} + \frac{128}{105} \mathcal{L}[\mathbf{E} \cdot \mathbf{E}] \right) + O(Ca^2). \quad (30)$$

$$\mathbf{F}^D = \frac{4}{3} Ca_S \mathcal{F}_0^D \mathbf{E} - \frac{4}{15} Ca_S \mathbf{E} + O(Ca^2). \quad (31)$$

Finally, the equation of the bubble surface can be expressed as

$$r = 1 + Ca_S (3\mathbf{F}^S : \mathbf{r} \mathbf{r} r^{-2}) + Ca_D (\mathcal{F}_0^D + 3\mathbf{F}^D : \mathbf{r} \mathbf{r} r^{-2}). \quad (32)$$

**APPENDIX E: GAS PRESSURE IN BUBBLE BASED ON SUFFICIENT
MACROSCOPIC PRESSURE ASSUMPTION**

Through dimensional analysis, the magnitude of the interface tension may not exceed the order of 10^4 N/m² when the bubble size is larger than 10 μ m. Meanwhile, the $O(1)$ viscous stress $4dR/Rdt$ in Eq. (19) is always less than the $O(Ca_S^{-1})$ interface tension due to the small deformation hypothesis. In these situations, even at a macroscopic pressure P as low as 1 atm (10^5 Pa), it is much larger than other terms on the right hand of the stress balance equation [Eq. (19)]. Hence, the pressure inside the bubble, p_g , can approximately equal to P , and

$$\nabla \cdot \mathbf{u}_g = -\frac{1}{P} \frac{dP}{dt}. \quad (33)$$

**APPENDIX F: SHEAR VISCOSITY OF BUBBLE SUSPENSIONS
CONSIDERING THE STRESS RELAXATION**

For Frankel's model [11] without considering the effect from dilatation motion, the constitutive equation with stress relaxation is expressed as

$$\langle \boldsymbol{\tau} \rangle + \frac{6}{5} Ca_S \frac{\mathcal{D} \langle \boldsymbol{\tau} \rangle}{\mathcal{D}t} = 2(1 + \phi_0) \langle \hat{\mathbf{e}} \rangle + Ca_S \left[\frac{12}{5} \left(1 - \frac{5}{3} \phi_0 \right) \frac{\mathcal{D} \langle \hat{\mathbf{e}} \rangle}{\mathcal{D}t} + \frac{48}{35} \phi_0 \mathcal{L} [\langle \hat{\mathbf{e}} \rangle \cdot \langle \hat{\mathbf{e}} \rangle] \right], \quad (34)$$

Under a steady simple shear flow that $\langle \mathbf{u} \rangle = (y, 0, 0)$, the relative shear viscosity given by Frankel's model [Eq. (34)] can be obtained that

$$\mu_r^F = 1 + \phi_0 \frac{1 - \frac{12}{5} Ca_S^2}{1 + \left(\frac{6}{5} Ca_S \right)^2} \quad (35)$$

To evaluate the real time contribution of the shear effect considered by Frankel and Acrivos [11], the initial void fraction ϕ_0 and the shear capillary number are replaced by ϕ and $Ca_S R$, respectively. Considering the viscosity of suspensions with spherical bubbles derived by Taylor [9], the pure shear induced viscosity $\Delta\mu_r^S$ can be expressed as

$$\Delta\mu_r^S = -\phi \frac{96 (Ca_S R)^2}{25 + 36 (Ca_S R)^2} \quad (36)$$

With the consideration of stress relaxation, the constitutive equation of the bubble sus-

pension we proposed [Eq. (13) in the main text] can be updated to

$$\begin{aligned} \langle \boldsymbol{\tau} \rangle + \frac{6}{5} Ca_S \frac{\mathcal{D} \langle \boldsymbol{\tau} \rangle}{\mathcal{D}t} &= 2(1 + \phi) \langle \hat{\mathbf{e}} \rangle + \frac{44}{15} \phi Ca_D \langle \hat{\mathbf{e}} \rangle \\ &+ Ca_S \left[\frac{12}{5} \left(1 - \frac{5}{3} \phi \right) \frac{\mathcal{D} \langle \hat{\mathbf{e}} \rangle}{\mathcal{D}t} + \frac{48}{35} \phi \mathcal{L} [\langle \hat{\mathbf{e}} \rangle \cdot \langle \hat{\mathbf{e}} \rangle] \right], \end{aligned} \quad (37)$$

where the rate of change of void fraction ϕ is related to the volumetric dilatation rate $\dot{\mathcal{V}}$, because

$$\phi = \frac{\frac{4}{3}\pi R^3}{\frac{4}{3}\pi R^3 + V_l}, \quad \text{and} \quad \frac{d\phi}{dt} = \phi \frac{3}{R} \frac{dR}{dt} + O(\phi^2) = -\phi \frac{1}{P} \frac{dP}{dt} + O(\phi^2), \quad (38)$$

where V_l is the liquid volume which is assumed to be a constant, and the $O(\phi^2)$ terms are neglected for the dilute system. Based on Eq. (38), $Ca_S d\phi/dt = \phi Ca_D$. To obtain the shear stress related to the viscosity, we should solve the following differential equations for the components of the deviatoric stress $\langle \boldsymbol{\tau} \rangle$:

$$\left(1 + \frac{6}{5} Ca_S \frac{\partial}{\partial t} \right) \tau_{11} - \frac{6}{5} Ca_S \tau_{12} = \frac{6}{5} \left(-1 + \frac{37}{21} \phi \right) Ca_S, \quad (39)$$

$$\left(1 + \frac{6}{5} Ca_S \frac{\partial}{\partial t} \right) \tau_{22} + \frac{6}{5} Ca_S \tau_{12} = \frac{6}{5} \left(1 - \frac{11}{7} \phi \right) Ca_S, \quad (40)$$

$$\left(1 + \frac{6}{5} Ca_S \frac{\partial}{\partial t} \right) \tau_{33} = -\frac{8}{35} \phi Ca_S, \quad (41)$$

$$\left(1 + \frac{6}{5} Ca_S \frac{\partial}{\partial t} \right) \tau_{12} + \frac{3}{5} Ca_S (\tau_{11} - \tau_{22}) = 1 + \phi + \frac{22}{15} \phi Ca_D. \quad (42)$$

where the time derivatives of the stress components τ_{ij} need to be taken into account due to the pressure changing with time. The analytical solutions of Eq. (34) corresponding to the pure shear flow [41] can be selected as the initial value ($t = 0$) of the set of differential equations of (39)-(42). Then we can obtain the value of the relative shear viscosity μ_r , which is equal to the value of the dimensionless shear stress τ_{12} . Finally, the dilatation induced viscosity $\Delta\mu_r^D$ can be calculated as $\mu_r - 1 - \Delta\mu_r^T - \Delta\mu_r^S$.

-
- [1] J. Rodríguez-Rodríguez, A. Sevilla, C. Martínez-Bazán, and J. M. Gordillo, Generation of microbubbles with applications to industry and medicine, *Annu. Rev. Fluid Mech.* **47**, 405 (2015).
- [2] B. Dollet, P. Marmottant, and V. Garbin, Bubble dynamics in soft and biological matter, *Annu. Rev. Fluid Mech.* **51**, 331 (2019).
- [3] D. J. Stein and F. J. Spera, Shear viscosity of rhyolite-vapor emulsions at magmatic temperatures by concentric cylinder rheometry, *J. Volcanol. Geoth. Res.* **113**, 243 (2002).
- [4] E. W. Llewellyn, H. M. Mader, and S. D. R. Wilson, The rheology of a bubbly liquid, *Proc. R. Soc. Lond. A* **458**, 987–1016 (2002).
- [5] H. M. Mader, E. W. Llewellyn, and S. P. Mueller, The rheology of two-phase magmas: A review and analysis, *J. Volcanol. Geoth. Res.* **257**, 135 (2013).
- [6] R. Zenit and J. J. Feng, Hydrodynamic interactions among bubbles, drops, and particles in non-newtonian liquids, *Annu. Rev. Fluid Mech.* **50**, 505 (2018).
- [7] A. Einstein, *Eine neue bestimmung der moleküldimensionen*, Ph.D. thesis, ETH Zurich (1905).
- [8] A. Einstein, Berichtigung zu meiner arbeit: Eine neue bestimmung der moleküldimensionen, *Ann. Phys.* **339**, 591 (1911).
- [9] G. I. Taylor, The viscosity of a fluid containing small drops of another fluid, *Proc. R. Soc. Lond. A* **138**, 41 (1932).
- [10] J. G. Oldroyd, The elastic and viscous properties of emulsions and suspensions, *Proc. R. Soc. Lond. A* **218**, 122 (1953).
- [11] N. A. Frankel and A. Acrivos, The constitutive equation for a dilute emulsion, *J. Fluid Mech.* **44**, 65 (1970).
- [12] H. A. Stone, Dynamics of drop deformation and breakup in viscous fluids, *Annu. Rev. Fluid Mech.* **26**, 65 (1994).
- [13] M. Manga, J. Castro, K. V. Cashman, and M. Loewenberg, Rheology of bubble-bearing magmas, *J. Volcanol. Geoth. Res.* **87**, 15 (1998).
- [14] M. Manga and M. Loewenberg, Viscosity of magmas containing highly deformable bubbles, *J. Volcanol. Geoth. Res.* **105**, 19 (2001).
- [15] A. C. Rust and M. Manga, Effects of bubble deformation on the viscosity of dilute suspensions,

- J. Non-Newtonian Fluid Mech. **104**, 53 (2002).
- [16] Y. M. Lim, D. Seo, and J. R. Youn, Rheological behavior of dilute bubble suspensions in polyol, Korea Aust. Rheol. J. **16**, 47 (2004).
- [17] S. W. Joh, S. H. Lee, and J. R. Youn, Rheological behavior of polydispersed bubble suspensions in shear flows, Polym. Eng. Sci. **1**, 128 (2010).
- [18] R. Morini, X. Chateau, G. Ovarlez, O. Pitois, and L. Tocquer, Steady shear viscosity of semi-dilute bubbly suspensions, J. Non-Newtonian Fluid Mech. **264**, 19 (2019).
- [19] S. Mitrou, S. Migliozi, P. Angeli, and L. Mazzei, Effect of polydispersity and bubble clustering on the steady shear viscosity of semidilute bubble suspensions in newtonian media, J. Rheol. **67**, 635 (2023).
- [20] K. Ohie, Y. Tasaka, and Y. Murai, Rheology of dilute bubble suspensions in unsteady shear flows, J. Fluid Mech. **983**, A39 (2024).
- [21] G. I. Taylor, The two coefficients of viscosity for an incompressible fluid containing air bubbles, Proc. R. Soc. Lond. A **226**, 34 (1954).
- [22] M. R. Islam and A. Chakma, Mechanics of bubble flow in heavy oil reservoirs, SPE Technical Paper **20070** (1990).
- [23] D. G. Fisher, J. Espidel, M. Huerta, L. Randall, and J. Goldman, Use of magnetic resonance imaging as a tool for the study of foamy oil behavior for an extra-heavy crude oil, Transp. Porous Media **35**, 189 (1999).
- [24] C. Or, K. Sasaki, Y. Sugai, M. Nakano, and M. Imai, Swelling and viscosity reduction of heavy oil by CO_2 -gas foaming in immiscible condition, SPE Res. Eval. Eng. **19**, 294 (2016).
- [25] W. J. Bergwerk, Flow pattern in diesel nozzle spray holes, Proc. Inst. Mech. Eng. **173**, 655 (1959).
- [26] W. H. Nurick, Orifice cavitation and its effect on spray mixing, J. Fluids Eng. (1976).
- [27] S. Tanveer and G. L. Vasconcelos, Time-evolving bubbles in two-dimensional stokes flow, J. Fluid Mech. **301**, 325 (1995).
- [28] C. Pozrikidis, Expansion of a compressible gas bubble in stokes flow, J. Fluid Mech. **442**, 171 (2001).
- [29] C. Pozrikidis, Computation of the pressure inside bubbles and pores in stokes flow, J. Fluid Mech. **474**, 319 (2003).
- [30] D. G. Crowdy, Compressible bubbles in stokes flow, J. Fluid Mech. **476**, 345 (2003).

- [31] G. K. Batchelor, The stress system in a suspension of force-free particles, *J. Fluid Mech.* **41**, 545 (1970).
- [32] R. G. Cox, The deformation of a drop in a general time-dependent fluid flow, *J. Fluid Mech.* **37**, 601 (1969).
- [33] H. Lamb, *Hydrodynamics*, 6th ed. (Cambridge U. Press, 1975) pp. 594–596.
- [34] L. Cifuentes, C. Dopazo, J. Martin, P. Domingo, and L. Vervisch, Local volumetric dilatation rate and scalar geometries in a premixed methane–air turbulent jet flame, *Proc. Combust. Inst.* **35**, 1295 (2015).
- [35] P. Abivin, I. Henaut, J. F. Argillier, and M. Moan, Rheological behavior of foamy oils, *Energy Fuels* **23**, 1316 (2009).
- [36] J. Sun, J. Jing, C. Wu, F. Xiao, and X. Luo, Pipeline transport of heavy crudes as stable foamy oil, *J. Ind. Eng. Chem.* **44**, 126 (2016).
- [37] Y. Lü, J. Han, L. He, X. Luo, S. Chen, and D. Yang, Flow structure and pressure gradient of extra heavy crude oil solution CO_2 , *Exp. Therm. Fluid Sci.* **104**, 229 (2019).
- [38] X. Wang, K. Li, and W. Su, Experimental and numerical investigations on internal flow characteristics of diesel nozzle under real fuel injection conditions, *Exp. Therm. Fluid Sci.* **42**, 204 (2012).
- [39] S. Ubertini, Injection pressure fluctuations model applied to a multidimensional code for diesel engines simulation, *J. Eng. Gas Turb. Power* **128**, 694 (2006).
- [40] A. J. McConnell, *Applications of Tensor Analysis* (Courier Corporation, 2014).
- [41] R. Pal, Rheological behavior of bubble-bearing magmas, *Earth Planet. Sci. Lett.* **207**, 165 (2003).